References

[1]Nicolai, L. M., *Fundamentals of Aircraft Design*, METS, Inc., San Jose, CA, 1975, pp. 18-2–18-5.

[2]McCormick, B. W., *Aerodynamics, Aeronautics, and Flight Mechanics*, Wiley, New York, 1979, pp. 344–346.

[3]Anon., "Generalized Method of Propeller Performance Estimation," United Aircraft Corp., Hamilton Standard Rept. PDB 6101A, Windsor Locks, CT, 1963.

[4]Raymer, D. P., *Aircraft Design: A Conceptual Approach*, AIAA Education Series, AIAA, Washington, DC, 1989, pp. 325–330.

Experimental Investigation of Vortex Breakdown over a Sideslipping Canard-Configured Aircraft Model

Sheshagiri K. Hebbar* and Max F. Platzer†
Naval Postgraduate School, Monterey, California 93943
and
Chang Ho Kim‡
Korean Air Force, Republic of Korea

Introduction

ALTHOUGH vortical flows dominate, the phenomenon of vortex breakdown (burst) and the onset of vortex asymmetry severely limit the high angle-of-attack (AOA) aerodynamics. When bursting is symmetric, only pitch stability is affected. When sideslip is present, the bursting becomes asymmetric, causing a rolling moment which adversely affects both roll and yaw stability. The effect of AOA on vortex bursting has been investigated extensively on delta wings,[1] and to a limited extent on complete aircraft configurations.[2–4] However, experimental data on the influence of sideslip on vortex bursting is limited,[5–7] and data on the effects of sideslip rate are still rather scarce even for simple wing shapes, let alone for complete aircraft configurations.

The canards affect the vortex development and have a strong influence on the lateral and directional stability.[8] The use of a close-coupled canard-configuration to achieve maneuverability and control in the poststall regime is the subject of growing scientific interest. Of special importance is the understanding of the vortex development and breakdown (bursting) under rapidly maneuvering conditions as envisioned for the U.S. Navy's X-31A aircraft. Therefore, an extensive, dye-injection flow-visualization study was undertaken in the Naval Postgraduate School (NPS) water tunnel, to characterize the vortical flowfield around a maneuvering canard-configured fighter aircraft model comparable to X-31A. The influence of canard location and pitch rate has been investigated earlier.[9,10] The results of the investigation on the effect of rate of sideslip are presented here. These *first* of a kind flow visualization results should be of interest to researchers working on similar configurations, especially in view of the clean support system used (Fig. 1). Additional details of the investigation appear in Refs. 11 and 12.

Received April 3, 1993; revision received June 21, 1993; accepted for publication July 6, 1993. This paper is declared a work of the U.S. Government and is not subject to copyright protection in the United States.

*Adjunct Professor, Department of Aeronautics and Astronautics. Associate Fellow AIAA.

†Professor, Department of Aeronautics and Astronautics. Associate Fellow AIAA.

‡Major.

Experimental Program

The NPS water tunnel is a horizontal, continuous flow, closed circuit facility with a test section 38 cm wide, 51 cm high, and 152 cm long. Water velocities of up to 30.5 cm/s are possible in the test section with a turbulence level of less than 1%. The dye-supply system for injecting color dyes through model ports consists of six pressurized color dyes using water soluble food coloring. The model support system, attached to the top of the test section, utilizes a C-strut to vary the pitch angle travel up to 50 deg, and a turntable to provide yaw variations up to ±20 deg (Fig. 1). Model pitch and yaw are controlled independently, with the yaw servo motor providing yaw rates of 1·8 deg/s and 2·8 deg/s.

The X-31A-like model used in this investigation is a simplified 2.3% scale model approximating the X-31A fighter aircraft with a double-delta wing, a delta-canard, a rectangular fuselage and several dye-injection ports (Fig. 2). The key dimensions of the model are: model length = 30.5 cm (12 in.), model span = 20.3 cm (8 in.), and wing root chord C_{wr} = 14.0 cm (5.5 in.). The canard's nondimensional location corresponded to $\bar{X}_c = X_c/C_{wr} = 43.18\%$, $\bar{Z}_c = Z_c/C_{wr} = 7.95\%$, where the canard's horizontal distance X_c and its vertical distance Z_c are measured from the quarter point of the canard root chord to the quarter point of the wing root chord.[10] The upper surface of the wing and the fuselage had grid lines marked for easy identification of vortex burst location.

The experimental program was carried out in two phases. The first phase involved the vortex flow visualization of the static model in the AOA range α = 15–50 deg at sideslip angles of β = 0, 5, 10, 15, and 20 deg. The second phase involved the dynamic vortex flow visualization of the sideslipping model for two rates of sideslip with β varying from 0 to 20 deg (simple sideslip increase motion) and 20 to 0 deg (simple sideslip decrease motion), both in the AOA range of 15 to 50 deg. The flow velocity in the water tunnel was nearly constant at 7.5 cm/s, corresponding to a nominal Reynolds number of 1.02×10^4 based on the wing root chord. The reduced yaw rates were $\dot{\beta}b/2U_\infty = 0.05$ and 0.08, where b is the model span, U_∞ is the freestream velocity, and $\dot{\beta}$ is the sideslip rate in rad/s. Note that these rates are comparable with the flight value of 0.03 for an assumed sideslip rate of 40 deg/s at 150 kt. The model yaw-axis was located at 62.7% of the wing root chord (21.5 cm aft of the nose). Extensive videotape recording and 35-mm photography of the model flowfield in both top view and side view were performed to document the observed flow phenomena during static and dynamic conditions.

Results and Discussion

All measurements were made on the *leeward* side of the model. Data reduction essentially consisted of measuring the burst location of the wing root vortex X_b from the leading edge of the wing root chord and plotting it as a function of AOA. The burst locations were determined from the photographs with the utmost care and consistency, and scaled for nondimensionalization using the wing root chord. Where necessary, videotape playback was used for clarification/confirmation of vortex burst location. Some degree of imprecision may be present in the reduced data due to the difficulty in locating the burst point, particularly at high angles of attack combined with high-rate dynamic motion. In addition, during the static segment of the experiment the burst location at any AOA was unsteady and fluctuated up to ±0.63 cm (i.e., about 4.5% of the wing root chord) about the mean location. For a discussion on the quality of NPS water tunnel burst data, see Hebbar et al.[4]

Figure 3 shows a typical asymmetric wing root vortex flow pattern at 20-deg AOA and 5-deg sideslip angle, with the vortex bursting on the leeward side at 75% of the wing root chord and lagging that on the windward side. The sideslip

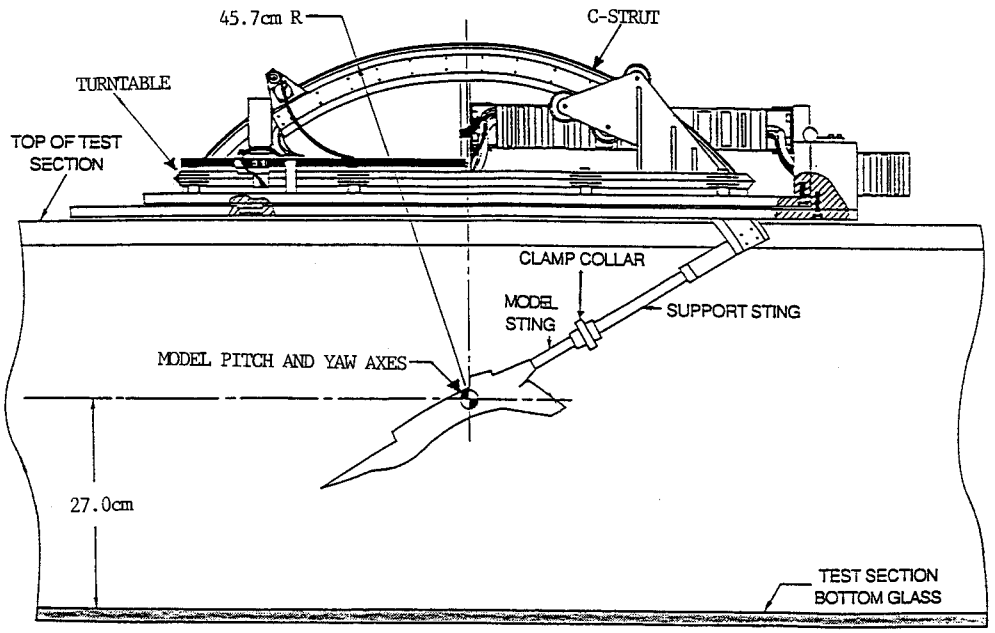

Fig. 1 Model support system of the NPS water tunnel.

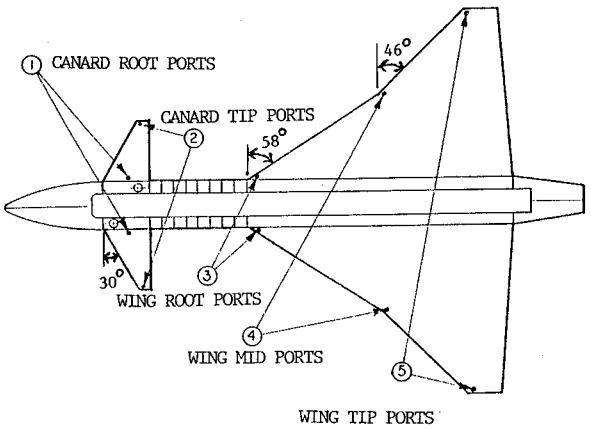

Fig. 2 2.3% scale model of X-31A-like aircraft with dye injection ports.

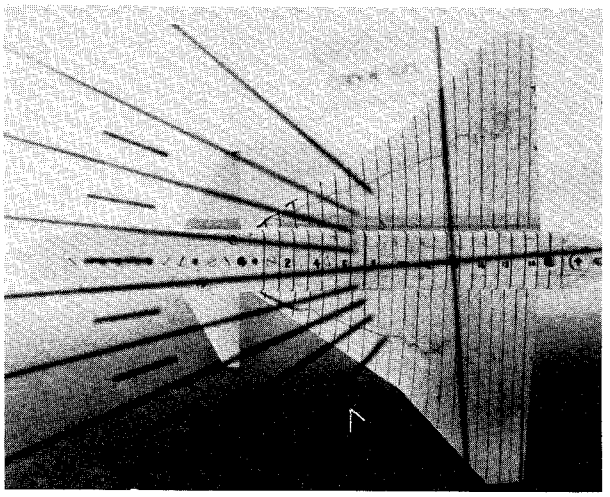

Fig. 3 Wing root vortex flow, static case, α = 20 deg, β = 5 deg.

plays a key role in the asymmetric development and bursting of wing root vortices, as has been demonstrated for a delta wing.[5] Reference 11 discusses these aspects in detail based on a careful examination of the static vortex flow patterns at different sideslip angles. At small sideslip angles (β = 5–10 deg) in the 15- to 20-deg AOA range, an asymmetric wing root vortex pair is seen to develop with the wing root vortex core bursting later on the leeward side than on the windward side. In the 25- to 30-deg AOA range, the vortices become symmetrical and burst at approximately the same location on both sides. However, in the 30- to 50-deg AOA range, the vortices become asymmetrical once again, but with the windward side vortex bursting later than the leeward side vortex. These effects on the bursting of leeward side vortex are shown quantitatively in Fig. 4. It is clear from the figure that the major effect of sideslip is to delay the vortex bursting on the leeward side throughout the AOA range tested (15–50 deg).

Figure 5 shows a typical asymmetric wing root vortex flow pattern at 20-deg AOA and 5-deg instantaneous sideslip angle, during positive sideslipping motion with a reduced yaw rate of $\dot{\beta}b/2U_\infty$ = 0.08. As seen here, the leeward side vortex is bursting later than the windward side vortex, but the amount of asymmetry is less than that in the corresponding static case (Fig. 3). This is attributed to the phenomenon of dynamic lag which causes an effective decrease in the leading-edge sweep

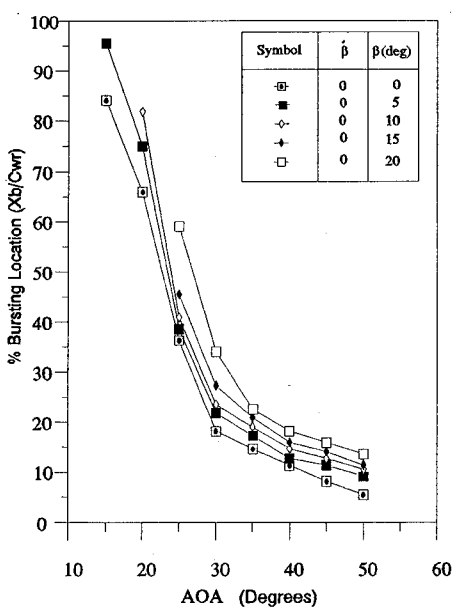

Fig. 4 Wing root vortex burst location as a function of AOA for static case at different sideslip angles (β = 0, 5, 10, 15, and 20 deg).

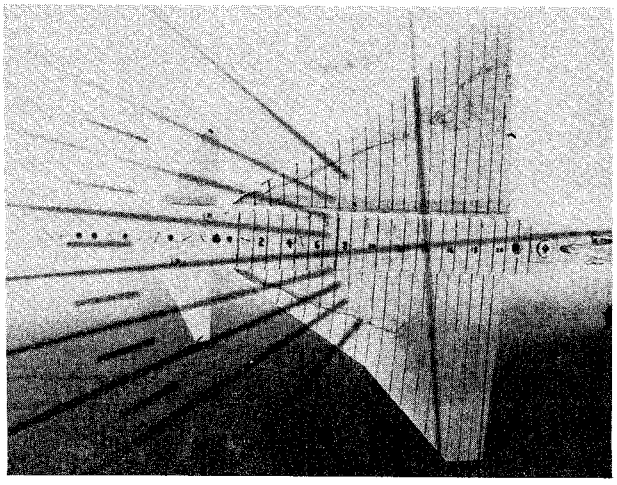

Fig. 5 Wing root vortex flow, dynamic case, α = 20 deg, β = 5 deg, $\dot{\beta}b/2U_\infty$ = 0.08.

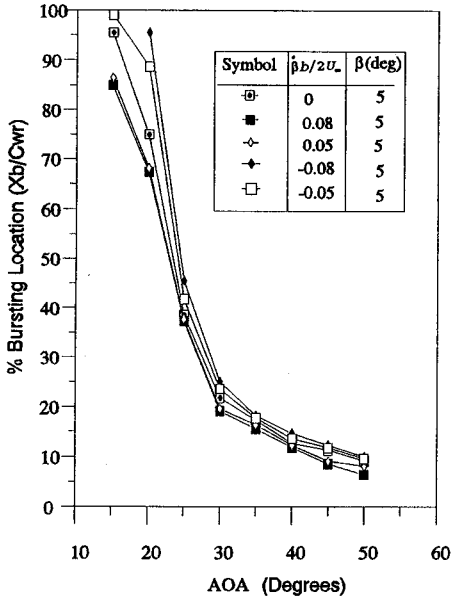

Fig. 6 Wing root vortex burst location at 5-deg instantaneous sideslip angle during sideslipping motion, as a function of AOA.

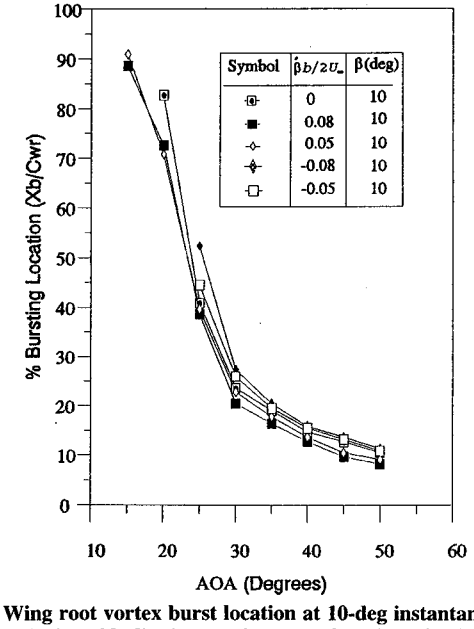

Fig. 7 Wing root vortex burst location at 10-deg instantaneous sideslip angle during sideslipping motion, as a function of AOA.

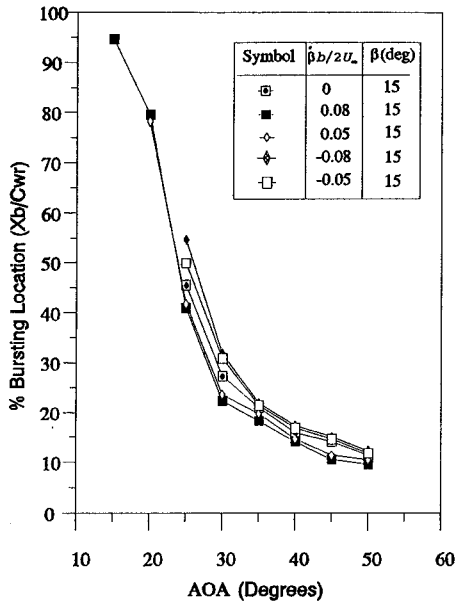

Fig. 8 Wing root vortex burst location at 15-deg instantaneous sideslip angle during sideslipping motion, as a function of AOA.

on the leeward side, and an effective increase on the windward side compared with the respective effective sweep angles in the static case. During the positive sideslipping motion, the vortex bursting on the leeward side occurs earlier than in the equivalent static case. Conversely, during the negative sideslipping motion, the vortex bursting on the leeward side occurs later than in the equivalent static case. Figures 6–8 show typical burst location plots highlighting the dynamic sideslip effects. These figures quantify the leeward side vortex burst response at instantaneous sideslip angles of 5, 10, and 15 deg, respectively. The corresponding burst location plot for the static case ($\dot{\beta}$ = 0) is also shown on these figures for purposes of comparison. Throughout the AOA range, it is seen that relative to the static case, the vortex burst on the leeward side always occurs earlier during the positive sideslipping motion, but later during the negative sideslipping motion. These dynamic lag effects are clearly seen to be a function of the reduced yaw rate (nondimensional sideslipping rate).

Conclusions

The following conclusions are drawn from the results of the investigation:

1) *Static sideslip effects*: vortex core bursting location is a function of sideslip angle. At a constant AOA, the leeward side vortex burst moves rearward and outboard with sideslip, and the windward side vortex burst moves forward and inboard. The vortex asymmetry switches sides as the AOA is increased (>30 deg).

2) *Dynamic sideslip effects*: during the positive/negative sideslipping motion, the leeward side vortex burst occurs earlier/later relative to the static case. The dynamic lag effects associated with sideslipping motion increase with the magnitude of the rate of sideslip.

Acknowledgments

This work was supported by the Naval Air Warfare Center/Aircraft Division, Warminster, PA, the Naval Air Systems Command, and the Naval Postgraduate School. The authors sincerely thank Alan McGuire for helping in the design and fabrication of the X-31A-like model.

References

[1]Lee, M., and Ho, C.-M., "Vortex Dynamics of Delta Wings," *Frontiers in Experimental Fluid Mechanics, Lecture Notes in Engi-*

neering, edited by M. Gad-el-Hak, Vol. 46, Springer-Verlag, Berlin, 1989, pp. 365–428.

[2]Brandon, J. M., and Shah, G. H., "Unsteady Aerodynamic Characteristics of a Fighter Model Undergoing Large Amplitude Pitching Motions at High Angles of Attack," AIAA Paper 90-0309, Jan. 1990.

[3]Del Frate, J. H., and Zuniga, F. A., "In-Flight Flow Field Analysis on the NASA F-18 High Alpha Research Vehicle with Comparisons to Ground Facility Data," AIAA Paper 90-0231, Jan. 1990; see also NASA TM 4193, May 1990.

[4]Hebbar, S. K., Platzer, M. F., and Cavazos, O. V., "Pitch Rate/Sideslip Effects on Leading-Edge Extension Vortices of an F/A-18 Aircraft Model," *Journal of Aircraft*, Vol. 29, No. 4, 1992, pp. 720–723; see also AIAA Paper 91-0280, Jan. 1991.

[5]Hummel, D., and Redeker, G., "Ueber den Einfluss des Aufplatzens der Wirbel auf die aerodynamische Beiwerte von Deltafluegeln mit klinen Seitenverhaeltnis beim Scheibeflug," Jahrbuch der W.G.L.R., 1967, pp. 232–240.

[6]Verhaagen, N. G., and Naarding, S. H. J., "Experimental and Numerical Investigation of Vortex Flow over a Sideslipping Delta Wing," *Journal of Aircraft*, Vol. 26, No. 11, 1989, pp. 971–978.

[7]Grismer, D., Nelson, R., and Ely, W., "An Experimental Study of Double Delta Wings in Sideslip," AIAA Paper 91-3308, Sept. 1991.

[8]O'Leary, C. O., and Weir, B., "The Effect of the Foreplanes on the Static and Dynamic Characteristics of a Combat Aircraft Model," AGARD-CP-465, Oct. 1989.

[9]Hebbar, S. K., Platzer, M. F., and Kwon, H. M., "Static and Dynamic Water Tunnel Flow Visualization Studies of a Canard-Configured X-31A-Like Fighter Aircraft Model," AIAA Paper 91-1629, June 1991.

[10]Hebbar, S. K., Platzer, M. F., and Kwon, H. M., "Vortex Breakdown Studies of a Canard-Configured X-31A-Like Fighter Aircraft Model," *Journal of Aircraft*, Vol. 30, No. 3, 1993, pp. 405–408.

[11]Kim, C. H., "Flow Visualization Studies of a Sideslipping, Canard-Configured X-31A-Like Fighter Aircraft Model," M.S. Thesis, Naval Postgraduate School, Monterey, CA, Dec. 1991.

[12]Hebbar, S. K., Platzer, M. F., and Kim, C. H., "Water Tunnel Visualization of Dynamic Effects During Sideslipping of a Canard-Configured Fighter Model," *Proceedings of the 5th Asian Congress of Fluid Mechanics* (Taejon, Korea), Vol. 2, 1992, pp. 1161–1164.

Comparing Aircraft Agility Using Mahalanobis Distances

John R. Howell*
Bradenton, Florida 34208
and
Norman E. Howell†
Edwards Air Force Base, California 93523

Introduction

IN a conversation among pilots, one might hear a statement to the effect that, considering agility, this airplane is "head and shoulders" above that one. The purpose of this Note is to show that such notions of distance can be quantified by use of the Mahalanobis generalized distance measure. Even though the presentation that follows is couched in terms of aircraft agility, the method is generally applicable.

Suppose a set of p agile maneuvers $X_1, X_2, \ldots, X_p$ is executed and measured N_1 times on an aircraft of one type, and N_2 times on an aircraft of another type, for a total of $N = N_1 + N_2$ p-variate measurements, all correlated and each measured in possibly different units. It is assumed that the errors of measurement are multivariate normal with equal covariance matrices. We want to calculate from these measurements a set of dimensionless distances D between the two aircraft for each of the p maneuvers, and for a linear compound of all the maneuvers.

In 1936 Mahalanobis[1] devised a generalized distance measure D defined by

$$D^2 = \boldsymbol{d}'S^{-1}\boldsymbol{d} \tag{1}$$

where $\boldsymbol{d}$ is a vector of differences between the p means, $\boldsymbol{d}'$ is the transpose of $\boldsymbol{d}$, and S^{-1} is the inverse of the pooled variance-covariance matrix S. Interest in and use of this distance measure continues, especially in India, to the present time. We note that the Mahalanobis distance is measured in a nonorthogonal p-dimensional space.

In the case where $p = 1$, D can be calculated easily from the equivalent relation

$$D^2 = [N(N-2)R^2]/[N_1N_2(1-R^2)] \tag{2}$$

where R is the sample correlation coefficient. For example, suppose the first aircraft performs one maneuver three times, and records the values 1, 2, and 3. The other aircraft performs the same maneuver three times and records the values 4, 5, and 6. We introduce a dummy variable y consisting of zeros for the first aircraft, and ones for the other aircraft, and display the data in two columns, as shown in Table 1.

We used a hand-held calculator, the Texas Instruments TI-35X, and entered the six data pairs in Table 1. With a single key-stroke, the calculator displayed the correlation coefficient $R = 0.87831$. Using Eq. (2) we got $D^2 = 9$. When there are p maneuvers, this simple procedure can be used to get a distance between the two aircraft for each one of the p maneuvers. The statistical significance of each of these distances can be checked by comparing the calculated R with a statistical table of R. Some of these values of R may be statistically nonsignificant, in which case one might be tempted to delete the data from that maneuver. However, this could be a mistake, because any distance measured, however small or statistically insignificant, may be highly suggestive, and therefore useful. For further discussions of the dangers of discarding correlated data, see Kramer[2] and Kendall.[3]

The defining relationship Eq. (1) can also be used to calculate D^2. From the data above, the mean difference $d = 5 - 2 = 3$. We calculated the pooled variance to be 1. Substituting in Eq. (1) we got $D^2 = 3 \times 1 \times 3 = 9$ as before. Either Eq. (1) or Eq. (2) may be used if we wish to calculate the distance between the two aircraft based on a linear compound (called a linear discriminant function) of the p measurements, and a computer already programmed for this is recommended. A superb choice is a stepwise buildup regression program (without an intercept estimate), which enters one variable at a time into the regression (namely that variable which most reduces the regression error) and prints a multiple

Table 1 Data for one maneuver

Dummy variable y	Maneuver X_1
0	1
0	2
0	3
1	4
1	5
1	6

Received March 11, 1993; revision received May 19, 1993; accepted for publication July 29, 1993.

*Associate Professor of Statistics, Retired, 519-23 Avenue East.
†Captain, USAF, Experimental Test Pilot.